



CHORUS

This is the accepted manuscript made available via CHORUS. The article has been published as:

Li intercalation at graphene/hexagonal boron nitride interfaces

Sharmila N. Shirodkar and Efthimios Kaxiras

Phys. Rev. B **93**, 245438 — Published 30 June 2016

DOI: [10.1103/PhysRevB.93.245438](https://doi.org/10.1103/PhysRevB.93.245438)

Li intercalation at graphene/hexagonal boron-nitride interfaces

Sharmila N. Shirodkar¹ and Efthimios Kaxiras^{1,2}

¹*John A. Paulson School of Engineering and Applied Sciences,
Harvard University, Cambridge, Massachusetts 02138, USA*

²*Department of Physics, Harvard University,
Cambridge, Massachusetts 02138, USA*

(Dated: June 6, 2016)

Abstract

Intercalation of Li in graphite and other layered structures is of interest for highly efficient energy storage devices. In this work, we determine the extent to which Li intercalates at the different interfaces formed between graphene (G) and hexagonal boron-nitride (hBN) heterostructures. We use ab-initio calculations to explore in detail the position of the dispersed Li atoms, changes in the structure at the interfaces, energetic stability of the configurations, and the corresponding electronic structure with varying concentrations of the intercalant. We trace the origin of the energetic stability and maximum concentration of Li that intercalates into various layered structures to the ability of the interface to accept electrons. Our calculations indicate that Li intercalates easiest at G/G interfaces, followed by interfaces between G/hBN, whereas Li cannot intercalate in hBN/hBN interfaces. Our results provide a framework for the design of experimental setups with optimal Li intercalation, and reveal the implications of intercalation on the dielectric properties of these materials and their possible application in plasmonics.

PACS numbers: 73.22.-f, 74.78.Fk, 74.62.Dh

The possibility of wide-spread use of clean energy sources has propelled research for the development of highly efficient energy storage devices. The rechargeable lithium ion battery is one such example of storage device with potential for high capacity and reliability¹. The performance of Li-ion based devices is determined by the electronic, structural and mechanical properties of the components that form the electrodes and those of the electrolytes. Graphite and non-graphitic carbon structures are at present the most commercially viable anode materials in these batteries². Carbon-based materials show reversible capacities of 450 mAh/g, with graphite delivering 372 mAh/g³. Advances in experimental methods are making it possible to build assemblies with one to few layers of graphene (G), and to explore their capability as anode electrodes. This level of structural control opens the possibility for large gains in the capacity and reliability of devices based on carefully engineered layered heterostructures. Recent experiments have successfully reported intercalation of Li in graphene bilayers^{4,5}, and one study has demonstrated that doping is also possible in heterostructures with graphene/hexagonal boron-nitride (hBN) interfaces⁴. To take advantage of the properties of these materials as negative electrodes in a Li battery, it is crucial to understand the intercalation/doping mechanism and the corresponding electronic structure of these layered assemblies. First-principles electronic structure calculations can determine the electronic and structural properties of these materials under controlled conditions which eliminate the effects of the ambient environment, side reactions, contamination and defects. Previous works studied the electronic and structural changes at different stages of Li intercalation in graphite⁶⁻⁸ and few-layer graphene⁹⁻¹². Park *et. al.*¹³ studied intercalation of metal atoms at the G/hBN interface, considered as an extrinsic defect at very low concentration of dopants. The inclusion of a large number of metal atoms between the van der Waals (vdW) bonded layers disrupts the nature of the interaction between layers and makes simple models unreliable in predicting their properties. A detailed theoretical understanding of the origin of the energetic and structural stability of intercalated structures, and the changes induced by intercalation to their electronic properties is necessary to guide further progress in the design of devices.

We have carried out detailed first-principles Density Functional Theoretical (DFT) calculations on bilayer G, bilayer hBN and G/hBN hetero-bilayers with varying concentration of Li to determine the effects of intercalation on the electronic and structural properties of these vdW-bonded layered structures. We determine the reaction potential and intercala-

tion energy (energetic stability) to estimate the maximum concentration of intercalated Li and hence the efficiency of graphene-based heterostructures anode materials in Li batteries. We used the Quantum ESPRESSO¹⁴ package, with plane-wave basis sets and ultrasoft pseudopotentials¹⁵ to represent the interaction between ionic cores and valence electrons. The exchange-correlation energy of the electrons is treated within the Generalized Gradient Approximated (GGA) functional of Perdew-Burke-Erzenhoff¹⁶. For the plane-wave basis we use an energy cutoff of 50 Ry for the wave functions and 600 Ry for the charge density. Structures were determined through minimization of the energy until the Hellmann-Feynman forces on each atom were smaller in magnitude than 0.03 eV/Å. To minimize the interaction between the periodic images along the direction perpendicular to the layers, we include a vacuum of approximately 20 Å. The semiempirical Grimme’s DFT-D2 functional¹⁷ was employed to include the vdW interactions between the layers.

The intercalation of Li atoms into heterostructures has been recently realized experimentally⁴, with G layers sandwiched between crystals of hBN to prevent sample degradation and to avoid side reactions. This arrangement implies that there exist 3 interfaces: G/G, G/hBN and hBN/hBN. We study Li intercalation at these three interfaces. In order to determine the ability of these interfaces to incorporate Li, we have carried out a detailed analysis of the energetic stability, electronic structure and local stability (structural changes) at varying concentrations of Li for the three interfaces. We have also examined how Li atoms are attached on a single layer of graphene, as a reference system.

The maximum Li concentration that can be achieved in bilayer graphene is LiC_{12} ($\sim 5 \times 10^{14} \text{ cm}^{-2}$), which corresponds to 1 Li atom in a $\sqrt{3} \times \sqrt{3}$ supercell⁴ of the graphene honeycomb lattice. In this work we have simulated a larger supercell ($2\sqrt{3} \times 2\sqrt{3}$), to study configurations with lower concentrations of Li doping Li_xC_{12} , with $x = 0.25, 0.5, 0.75, 1, 1.25$ and 1.5 . The Brillouin zone integrations were carried over $6 \times 6 \times 1$ Monkhorst-Pack¹⁸ set of k-points for structural relaxation, while we used a denser $18 \times 18 \times 1$ Monkhorst-Pack set of k-points in calculating the Bader charges. At each concentration, there exist several possible positions for Li intercalation in the bilayer. We only considered the symmetrically inequivalent configurations at each concentration in the $2\sqrt{3} \times 2\sqrt{3}$ supercell, which were generated using the Site Occupancy Disorder (SOD) program^{19,20}. For the G bilayer, the number of inequivalent configurations were 1, 4, 3, 2, 2 and 2 for $x = 0.25, 0.5, 0.75, 1, 1.25$ and 1.5 , respectively; these numbers for the hBN bilayer are 1, 4, 4 and 2, and for the G

monolayer 1, 4, 3 and 2, at $x= 0.25, 0.5, 0.75$ and 1, respectively. Since the G/hBN heterostructure does not possess inversion symmetry, it has the largest number of inequivalent configurations, 2, 12, 6 and 2 for $x= 0.25, 0.5, 0.75$ and 1, respectively. Amongst all the symmetrically inequivalent configurations, we henceforth limit our discussions only to the energetically most stable configuration at each concentration.

To estimate the energetic stability of the different configurations, we determined the intercalation energy per Li atom (E_I) and the reaction potential (E_R). E_R is the average potential for extracting Li from a material. E_I and E_R are defined as

$$E_I = \frac{1}{n} [E(\text{Li}_n\text{M}) - E(\text{M}) - nE(\text{Li})], \quad (1)$$

$$E_R = -\frac{1}{y-x} [E(\text{Li}_y\text{M}) - E(\text{Li}_x\text{M}) - (y-x)E(\text{Li})], \quad (2)$$

where, $E(\text{Li}_x\text{M})$ is the energy of Li intercalated with concentration x in M [for the G/G structure, $\text{M} = \text{C}_{12}$, for hBN/hBN, $\text{M} = (\text{BN})_6$, for G/hBN, $\text{M} = \text{C}_6(\text{BN})_3$], $E(\text{Li})$ is the energy of a Li atom in bulk Li, and n is the number of Li atoms. The configuration is stable if both conditions, $E_I < 0$ and $E_R > 0$, are satisfied.

We consider first intercalation between two graphene layers. The properties of graphene multilayers depend on the stacking sequence, which can impact the intercalation of Li in these structures. To study the effect of Li intercalation on the stacking of the bilayers, we have considered both *AA* and *AB* stacking for all interfaces (see Fig. 1). In Fig. 2 we show the intercalation energy and reaction potential for graphene bilayer, as well as the Li-layer separation ($d/2$, which is half of the interlayer separation d) with concentration of Li atoms for both stacking sequences. Our results clearly indicate that the *AA* stacked layers of graphene are energetically more favourable for Li intercalation. The LiC_{12} ($x= 1$) configuration in *AA* stacking is 0.3 eV energetically more stable than *AB* stacking. The structural relaxation of the graphene bilayer with Li for $x>1$, indicates that the two layers get displaced relative to each other to achieve *AA* stacking¹¹, even though the pure graphene bilayer is most stable in the *AB* stacked structure. The energetic stability of the *AA* stacked intercalated bilayer is due to the fact that Li atoms occupy the hollow sites between the layers in *AA* stacking^{9,10}, which decreases the interlayer separation d (as compared to *AB* stacking) and lowers the energy (see Fig. 2). We shall henceforth restrict our discussion to

AA stacked graphene interfaces.

The concentration up to which Li intercalates in the graphene bilayer can be traced to the amount of charge transferred from Li into the monolayers. Since graphene is not an insulator, the charge donated by the Li atom gets equally distributed between the two layers. Our Bader charge analysis shows that $0.88 \bar{e}$ per Li atom is transferred from Li to the graphene layers (in agreement with previous reports¹⁰). The interlayer separation (d) increases with the concentration of Li atoms, up to 3.7 \AA for $x= 1$ ²¹ compared to 3.3 \AA for the AA stacked bilayer with no intercalation^{22,23}. As the graphene layers get doped, the Fermi level shifts from the Dirac point into the conduction band as seen in the density of states (DOS), Fig. 1(c). For concentrations higher than $x= 1$, the configurations become energetically unstable mostly due to the repulsion between the positive Li ions⁹ and the inability of the graphene layers to accept more charge. This is referred to as Pauli blocking in Raman spectra⁴. This instability is manifested by a negative reaction potential or positive intercalation energy. The reaction potential for $x= 1.25$ and $x= 1.75$ is zero within the accuracy of our calculations.

We consider next intercalation between graphene and hBN layers. Since there are three elements (C, B and N) in this hetero-bilayer, there are two ways to stack the layers to achieve AB stacking: C on top of B or C on top of N. We simulated the AB stacked bilayer with B directly below C and N in the hollow site of the graphene hexagon, Fig. 1(f), since it is the most stable configuration²⁴ for the G/hBN interface. Our results show that, similar to graphene bilayers, AA stacking is energetically more favourable than AB stacking by 0.1 eV for $x= 1$ ($\text{LiC}_6(\text{BN})_3$). Compared to the graphene bilayer, AB stacking here is less unfavorable mostly because the C atom does not directly bind to the Li. The maximum concentration of Li is $x= 0.25$, $\text{Li}_{0.25}\text{C}_6(\text{BN})_3$ or $1.3 \times 10^{14} \text{ cm}^{-2}$. A lower amount of Li intercalates in G/hBN hetero-bilayer which is explained by the following observations: electrons from Li are first transferred into graphene up to concentrations of $x= 0.25$, or up to $0.88 \bar{e}$ per Li atom. Beyond $x= 0.25$, Li starts donating electrons to the hBN layer, which causes the system to destabilize since hBN is an insulator and does not prefer the transfer of charge. Similar to the graphene bilayer, the interlayer separation increases with increasing Li concentration up to 3.5 \AA , compared to 3.3 \AA for the undoped hetero-bilayer²⁵. The DOS (see Fig. 1(h)) shows doping up to $E_F \approx 1.0 \text{ eV}$ for $x= 0.25$, which is in good agreement with experimental findings by Elbaz *et. al*⁴, leading to Pauli blocking of the graphene layer due to sufficient Li intercalation.

We next consider the case of hBN bilayer, to examine the possibility of Li intercalation in the pacifying layers. Since our calculations on the graphene bilayer and the G/hBN heterostructure clearly indicate that *AA* stacking is preferred for Li intercalation, we have restricted ourselves to calculations of the *AA* stacked bilayer hBN. The energetics (see Fig. 2) clearly show that Li does not intercalate into the hBN bilayer for $x \geq 0.25$. This is because each Li transfers $0.88 \bar{e}$ of charge into the hBN layer, and since hBN is an insulator the configuration becomes unstable. Here again the interplanar separation increases as the Li concentration increases (see Fig. 2). Li may intercalate into this bilayer but the amount of intercalation will be negligible compared to the amount in G layers or G/hBN interfaces.

In order to estimate the amount of charge transferred by Li into a single layer of graphene, a useful reference structure, we also carried out a systematic study of the adsorption energy (E_A) and reaction potential with varying concentration of Li on a graphene monolayer. None of the symmetry inequivalent configurations show energetically favorable adsorption⁹ at any concentration of Li (see Fig. 2). This suggests that though Li intercalates favorably in bilayers with one or both layers being graphene (the G/G or G/hBN systems), single layer graphene is unfavorable for adsorption of Li at $x \geq 0.25$. Lee *et. al.*⁹ also reported no absorption of Li on monolayer graphene. The Li-graphene distance increases from 1.75 \AA to 1.87 \AA in going from $x=0.25$ to $x=1$ (see Fig. 2). Interestingly, the charge transfer decreases from $0.9 \bar{e}$ to $0.66 \bar{e}$ (in agreement with Ref.¹⁰) in going from $x=0.25$ to $x=1$, whereas in any of the intercalated bilayers a fixed amount of charge ($0.88 \bar{e}$ per Li) is transferred into graphene irrespective of the Li concentration. We note that Li can adsorb on defective graphene layers by binding to dangling bonds at carbon vacancies or unpassivated edges⁹.

We turn to a different aspect of the intercalated bilayers, namely their dielectric properties. Depending on the behavior of its dielectric function with frequency, a material can have interesting applications in capacitive or plasmonic devices. The dielectric function is a complex quantity, with the real part (ϵ_R) representing the polarizability and the imaginary part (ϵ_I) representing the energy dissipated in the material. A more positive real part at zero frequency (the static dielectric constant) leads to larger capacity of the material to store charge. A negative real part of dielectric function represents the capability of the material to support plasmons. The lifetime and the propagation length of the plasmon is governed by the losses, that is, the imaginary component of the dielectric function. The usual requirement for plasmonic devices is a reduction of losses and the ability to fine tune the plasmon

frequency by making the real part of the dielectric function negative at a given frequency.

To understand the effect of intercalation on the dielectric properties, we carried out calculations of the pure structures and those with doping of the same level as in the systems discussed here, but restricted to a primitive unit cell of the pure system to circumvent the computational cost of larger supercells (details will be discussed in a separate paper). The comparison between dielectric functions of the doped G bilayer, the monolayer graphene and the G/hBN bilayer at appropriate relaxation times of 34.2 fs and 101 fs for bilayer and monolayer graphene²⁶, reveals that conduction electrons transferred from Li give rise to a Drude peak with negative ϵ_R for frequencies in the IR and visible range, suggesting the possibility of potential applications in plasmonic devices. We note that due to interaction between the layers in bilayered or multi-layered systems, the the relaxation time is smaller which gives rise to larger losses (confirmed by our calculations). In Fig. 3 the straight orange line drawn at -30 cuts ϵ_R at 520 THz, 260 THz, 345 THz and 124 THz for the AA stacked G/G, G/hBN, and monolayer graphene with doping concentration same as that of a single layer in G/G labeled G1, and in G/hBN hetero-bilayer labeled G2. Though the frequency increases with the doping concentration, ϵ_I at these frequencies is 5.0, 4.2, 2.2, 8.4 for G/G, G/hBN, G1 and G2, indicating larger losses in bilayers. This implies that stacking of layers intercalates more Li and increases the plasma frequency, however losses increase due to smaller relaxation times, and hence reduce the efficiency of the plasmonic device. One possible way to overcome this drawback will be to suppress the scattering of electrons by adjacent layers by increasing the interlayer separation (which corresponds to reducing the interlayer interaction), by changing the stacking sequence or by insertion of non-interacting spacers. These findings can guide experimental realizations of electronic and plasmonic devices based on the Li-intercalated G/G and G/hBN structures.

Acknowledgements

We thank Frank Zhao, Giselle Elbaz, Bedaiko Kwabena and Philip Kim for useful discussions of experimental results. We acknowledge support by ARO MURI Award No. W911NF14-0247. For the computations the odyssey cluster of the Research Computing Group at Harvard University, and the Extreme Science and Engineering Discovery Environment (XSEDE), which is supported by NSF Grant No. ACI-1053575.

Figures

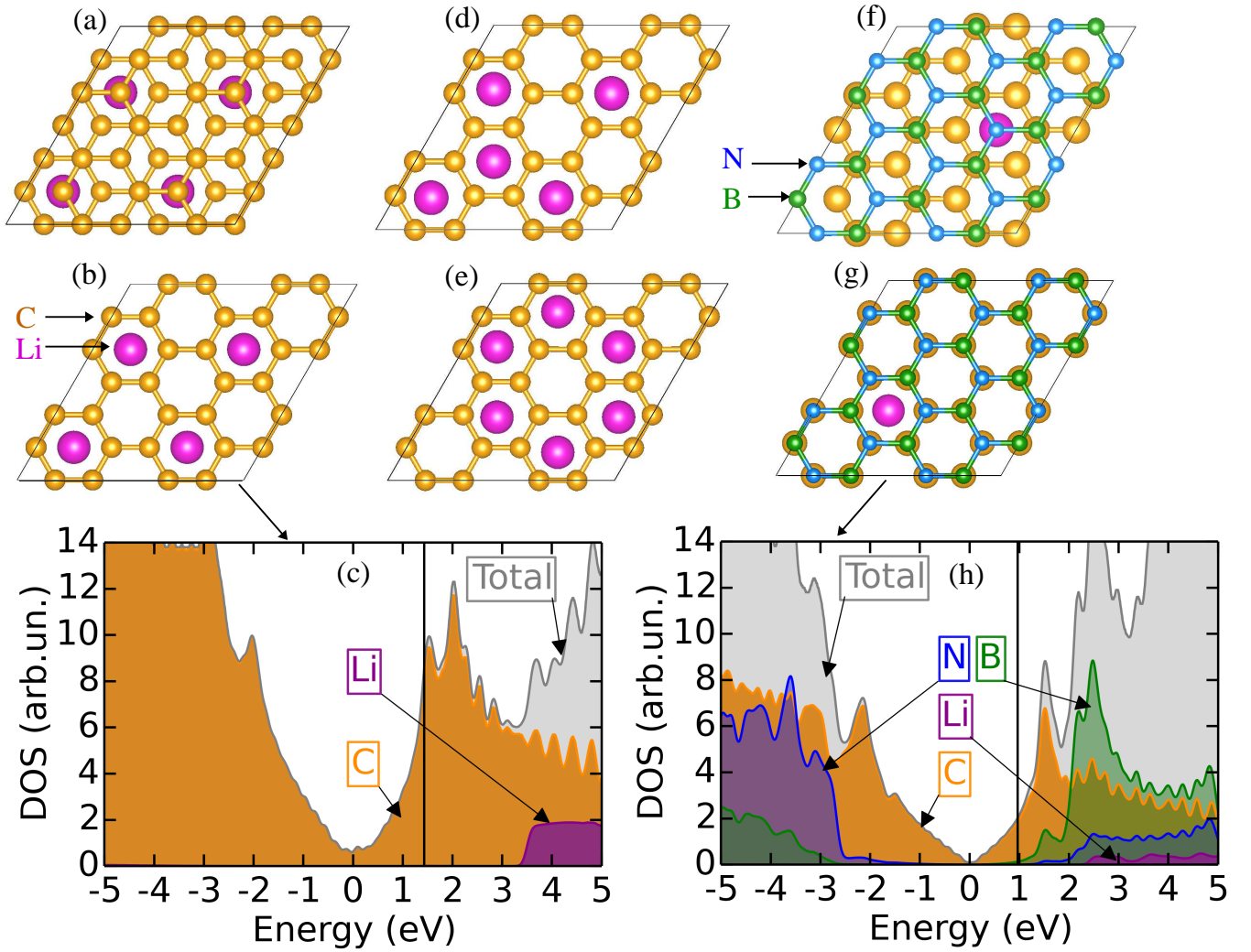


FIG. 1. Relaxed structures of (a) *AB* stacked and (b) *AA* stacked bilayer graphene with Li intercalation concentration $x=1$ ($\text{Li}_{x=1}\text{C}_{12}$). (c) Density of states projected unto the atomic orbitals for *AA* stacked configuration at maximum intercalation concentration ($x=1$). Note that, E_F lies ≈ 1.5 eV above Dirac point (black vertical line). (d), (e): most stable *AA* stacked graphene bilayer configurations for $x=1.25$ and $x=1.5$. (f) *AB* stacked and (g) *AA* stacked relaxed structure of graphene/h-BN with Li intercalation concentration, $x=0.25$ ($\text{Li}_{0.25}\text{C}_6(\text{BN})_3$). (h) Density of states projected onto the atomic orbitals for *AA* stacked configuration at maximum intercalation concentration ($x=0.25$). E_F lies ≈ 1.0 eV above Dirac point (black vertical line).

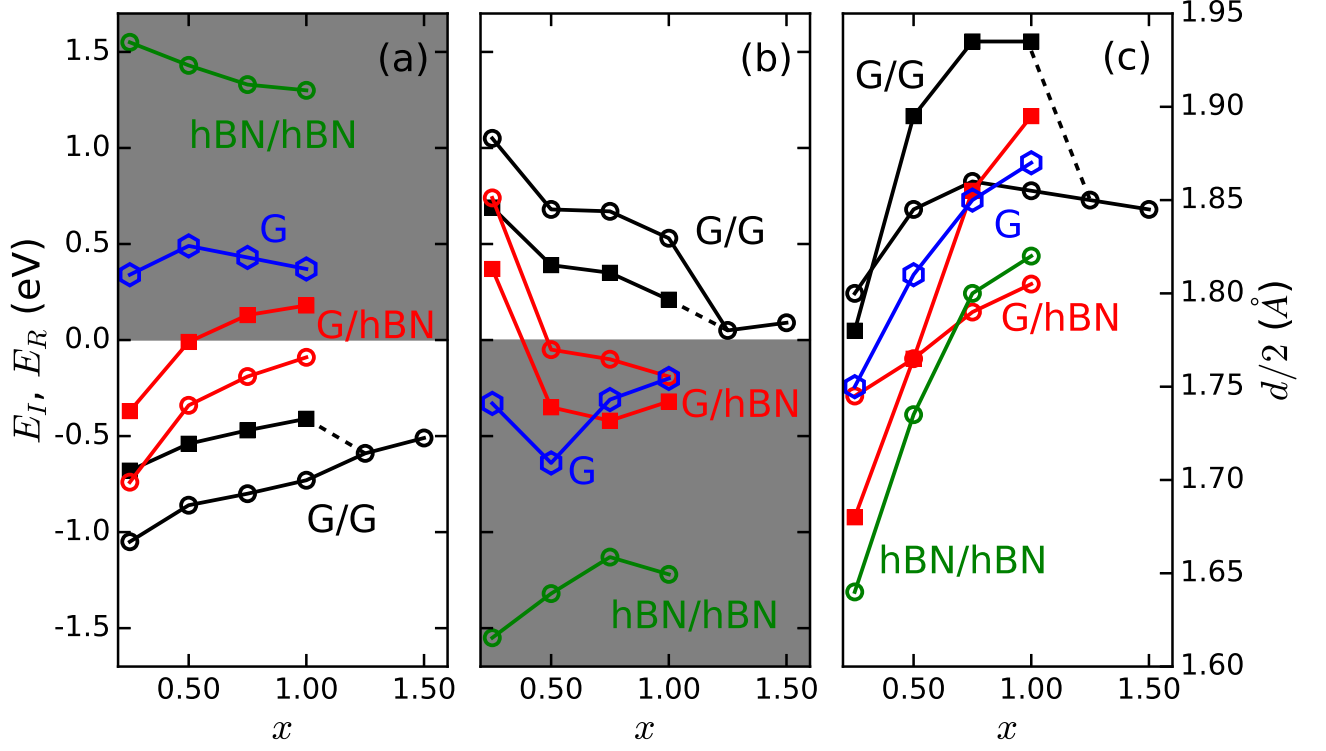


FIG. 2. (a) Intercalation energy (E_I in eV), (b) reaction potential (E_R in eV), and (c) Li-layer separation ($d/2$ in Å) for graphene bilayer (G/G in black), graphene-hexagonal boron-nitride (G/hBN in red), hexagonal boron-nitride bilayer (hBN/hBN in green) in the AA (open circles) and AB (filled squares) stacked configurations, and monolayer graphene (G in blue). Areas shaded in grey indicate regions of energetically unstable states, and the dashed lines represent the switch from AB stacking to AA stacking in G/G.

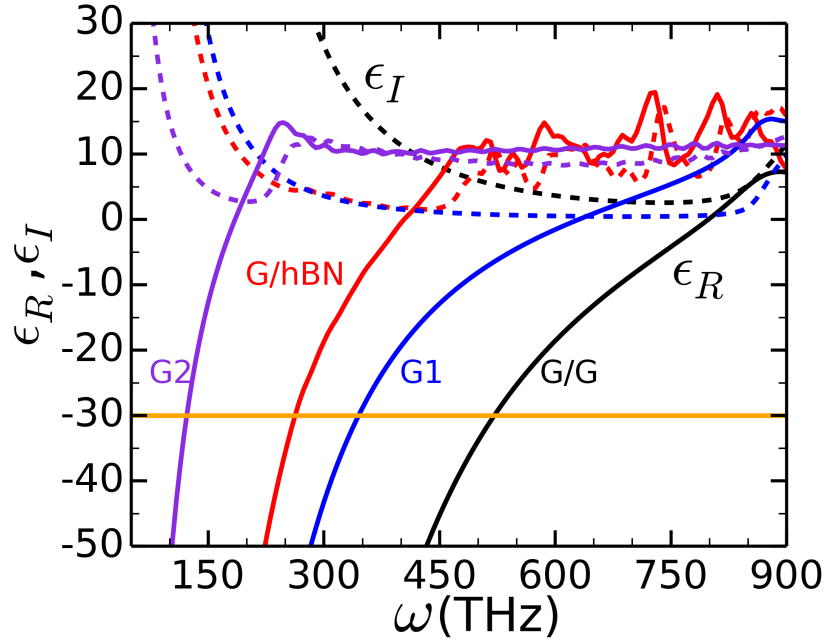


FIG. 3. Dielectric function real and imaginary parts (ϵ_R, ϵ_I) of bilayer graphene (G/G, black lines), graphene/hBN hetero-bilayer (G/hBN, red lines), monolayer graphene with doping concentration same as in bilayer graphene (G1, blue lines), and same as in graphene/hBN hetero-bilayer (G/hBN, violet lines).

-
- ¹ M. S. Islam and C. A. Fisher, *Chemical Society Reviews* **43**, 185 (2014).
- ² M. Noel and V. Suryanarayanan, *Journal of Power Sources* **111**, 193 (2002).
- ³ J.-M. Tarascon and M. Armand, *Nature* **414**, 359 (2001).
- ⁴ E. Giselle, Z. Frank, and K. Philip, In preprint (2016).
- ⁵ K. Sugawara, K. Kanetani, T. Sato, and T. Takahashi, *AIP Advances* **1**, 022103 (2011).
- ⁶ K. Persson *et al.*, *Phys. Rev. B* **82**, 125416 (2010).
- ⁷ S. Thinius, M. M. Islam, P. Heitjans, and T. Bredow, *The Journal of Physical Chemistry C* **118**, 2273 (2014).
- ⁸ E. Hazrati, G. A. de Wijs, and G. Brocks, *Phys. Rev. B* **90**, 155448 (2014).
- ⁹ E. Lee and K. A. Persson, *Nano Letters* **12**, 4624 (2012), pMID: 22920219.
- ¹⁰ D. Guzman, H. Alyahyaei, and R. Jishi, *2D Materials* **1**, 021005 (2014).
- ¹¹ J. Zhou *et al.*, *Science China Physics, Mechanics and Astronomy* **55**, 1376 (2012).
- ¹² X. Shao, K. Wang, R. Pang, and X. Shi, *The Journal of Physical Chemistry C* **119**, 25860 (2015).
- ¹³ S. Park, C. Park, and G. Kim, *The Journal of Chemical Physics* **140**, (2014).
- ¹⁴ P. Giannozzi *et al.*, *Journal of Physics: Condensed Matter* **21**, 395502 (2009).
- ¹⁵ D. Vanderbilt, *Phys. Rev. B* **41**, 7892 (1990).
- ¹⁶ J. P. Perdew, K. Burke, and M. Ernzerhof, *Physical Review Letters* **77**, 3865 (1996).
- ¹⁷ S. Grimme, *Journal of computational chemistry* **27**, 1787 (2006).
- ¹⁸ H. J. Monkhorst and J. D. Pack, *Phys. Rev. B* **13**, 5188 (1976).
- ¹⁹ R. Grau-Crespo, S. Hamad, C. R. A. Catlow, and N. H. de Leeuw, *Journal of Physics: Condensed Matter* **19**, 256201 (2007).
- ²⁰ R. Grau-Crespo and U. Waghmare, (CRC Press, ADDRESS, 2012), Chap. Simulation of Crystals with Chemical Disorder at Lattice Sites, pp. 303–326, 0.
- ²¹ K. Persson *et al.*, *Phys. Rev. B* **82**, 125416 (2010).
- ²² M. Birowska, K. Milowska, and J. Majewski, *Acta Phys Pol A* **120**, 845 (2011).
- ²³ A. M. Popov *et al.*, *The Journal of Chemical Physics* **139**, (2013).
- ²⁴ Y. Sakai, T. Koretsune, and S. Saito, *Phys. Rev. B* **83**, 205434 (2011).
- ²⁵ A. M. Ukpong, *Computational Condensed Matter* **2**, 1 (2015).

²⁶ I.-T. Lin *et al.*, Physical Review B **86**, 235446 (2012).